Determination of Space Object Size in LEO using Measurement of Brightness

Seda Aydın
TUBITAK Space Technologies Research Institute
Ankara, Türkiye
ORCID : 0000-0002-3128-5390

Muhammed Selim Atar
TUBITAK Space Technologies Research Institute
Ankara, Türkiye
selim.atar@tubitak.gov.tr

Mehmet Ali Arabacı
TUBITAK Space Technologies Research Institute
Ankara, Türkiye
ORCID : 0000-0002-5433-5864

Murat Gökçe
TUBITAK Space Technologies Research Institute
Ankara, Türkiye
murat.gokce@tubitak.gov.tr

Taha Muharrem Lahaçlar
TUBITAK Space Technologies Research Institute
Ankara, Türkiye
taha.lahaclar@tubitak.gov.tr

2023 10th International Conference on Recent Advances in Air and Space Technologies (RAST) | 979-8-3503-2302-3/23/$31.00 ©2023 IEEE | DOI: 10.1109/RAST57548.2023.10197958

***Abstract*— The growing number of satellites and space debris in Earth's orbit is a significant concern for space traffic. Therefore, numerous observation systems on the ground and in space constantly track space objects. Considering that the fragmentation of space debris over time poses a risk to orbit, the size of objects should be determined to assess their potential impact. In this study, we observed one of the known satellites, SJ-6F, using passive ground-based optical systems in different locations. After that, the conjugate sphere radius of SJ-6F was estimated from the apparent brightness data, which was extracted from optical observations. Finally, it was compared with its actual dimensions. The results clearly showed the effectiveness of the proposed solution since the estimated (0.356 meters) and known radius (0.327 meters) of the satellite were very close to each other.**

Keywords—apparent magnitude, low earth orbit, satellites, space debris, space object's size, Space Situational Awareness

I. INTRODUCTION

The increasing number of satellites and space debris in Earth's orbit has led to growing concerns about space traffic management. The crowded space environment poses a risk to operational satellites and spacecraft, and collisions with space objects can have severe consequences. To mitigate these risks, it is essential to monitor and track space objects continuously and analyze their characteristics. This information is critical for predicting potential collisions and taking preventive measures. Therefore, numerous observation systems on the ground and in space track space objects' orbits and characteristics, such as size, shape, and composition. The data collected from these observations enable researchers to assess the potential impact of space objects and develop mitigation strategies.

The determination of an average satellite's size using apparent magnitude, range, and phase angle is accomplished using photometry. Photometry involves measuring the brightness of a celestial object (in this case, a satellite) and using that information to determine various physical characteristics, such as its size and reflectivity.

The apparent magnitude of a satellite is measured using a photometer, an instrument that measures the amount of light emitted by an object. The range of the satellite can be determined using radar or other distance-measuring techniques. The phase angle is the angle between the sun, the observer, and the satellite and can be calculated using basic trigonometry.

Photometry can be utilized to derive the physical characteristics of celestial objects (in our case, a satellite), such as their sizes and reflectivity, by measuring their apparent magnitudes. The apparent magnitude of a satellite is measured using a photometer, an instrument that measures the amount of light emitted by an object. To be able to extract physical information of satellites, we should also have the range and phase angle information. While radars or other distance-measuring techniques can provide the range of a satellite, basic trigonometry is employed to calculate its phase angle, which is the angle between the sun, the observer, and the satellite.

Numerous studies are being carried out to determine the size and shape of satellite and space debris from their light curves. Size analyses can also be estimated through modeling in laboratory conditions in addition to observations. Brightness analyses can vary depending on the type of orbit. Krantz et al. [1] analyzed 14,000 observation data for Starlink and Oneweb satellites in LEO and found that at least 5 observation data were required for the photometric signature to be confirmed with an accuracy of 80%. Brightness analysis is specialized for satellites with large phase angles observed in GEO [2]. Assumptions are made for certain parameters in observations. The celestial body is characterized and classified by assigning a size based on simple shapes such as spheres or cylinders [3] or the type of celestial body, such as bodies, payloads, and debris [4]. Detailed studies have been carried out to obtain information about the size of the satellite from the relationship between the observed brightness and the phase angle of the satellite [5]. Additionally, attitude analysis can be made from the brightness change of the satellite in orbit [6], [7]. Material-type of the observed celestial body can be analyzed with spectral observations [8], [9]. Since the brightness can vary depending on the material used in the celestial body, studies are also carried out under laboratory conditions at different phase angles to examine the size of the

observed celestial body [10], [11]. The results of the size estimation are improved using Lambertian spherical phase angle correction [12]. In this study, size analysis was performed based on the published brightness of the satellite and space debris assuming an albedo value is 0.1 and a spherical shape using modeled brightness calculation [13]. The deviation of the observed brightness from the calculated brightness was examined by observing a single satellite with different optical systems on the same and different nights and from different observation sites, considering the effect of different optical systems and light pollution at the observation site [14], [15].

II. METHOD

The proposed method is composed of four phases, as shown in Fig. *1*. Firstly, image processing techniques were employed to segment star and satellite objects in images. Secondly, segmented stars were registered with the stars of a pre-defined star catalog using astrometric analysis. After that, the brightness of the detected satellites was computed proportional to the apparent magnitudes of the registered stars. Finally, the sizes of the detected satellites were estimated using their apparent magnitudes.

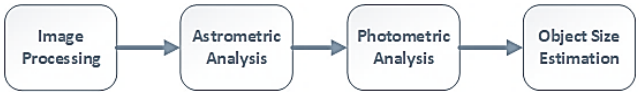

Fig. 1. The proposed solution for object size estimation

A. Image Processing

It is better to mention the image processing techniques used to segment celestial objects in images before proceeding to the astrometric and photometric analysis. Fig. *2* shows a sample image, including a satellite that belongs to Low Earth Orbit (LEO). The target satellite was observed as a line (shown in the blue circle) and the stars as point light sources because of short exposures (around 100 msec).

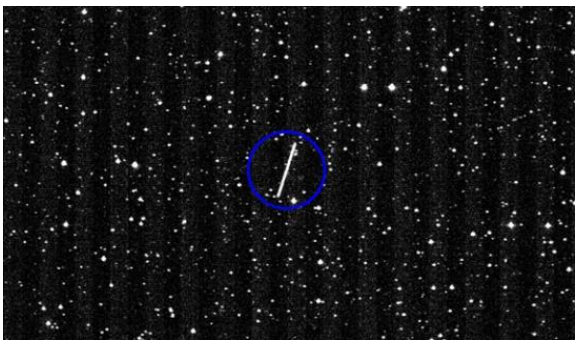

Fig. 2. Detection of space object in LEO

The aim of image processing is to segment star and satellite objects in the image plane precisely. We first extracted a background map from the images using well-known image processing techniques (e.g., adaptive thresholding and connected component analysis). After that, the segmented objects were labeled as stars or satellites according to their morphological properties (i.e., categorizing circular objects as stars and line-shape objects as satellites). We also needed to extract the centroids of stars from segmented pixels to use in the astrometric analysis later. For that purpose, the weighted average of segmented stars was computed with the help of the spatial moments along (x,y) dimensions in the image plane. On the other hand, the brightness of the detected space objects (stars and satellites) in images was calculated using their average pixel intensities over the segmented areas.

To realize the image processing pipeline of this study, we utilized the various functions of the OpenCV (v3.2.0) [16] library to perform pre-processing, object segmentation, brightness calculation, and centroid estimation steps.

B. Astrometric Analysis

Astrometry is the branch of astronomy that involves precise measurements of the positions and motions of celestial objects such as stars, planets, asteroids, and comets. It is concerned with measuring the coordinates (position and motion) of these objects in the sky and their changes over time, which is crucial for studying the structure and evolution of the universe. Astrometry is also used to determine the angular position of objects in the Earth's orbit.

In our work, we utilized astrometry to determine the attitude of the given image with the help of the centroids of stars. The centroid points in the image plane were compared with a reference star catalog (UCAC4 [17]) based on the quad-matching algorithm [18] shown in Fig. *3*.

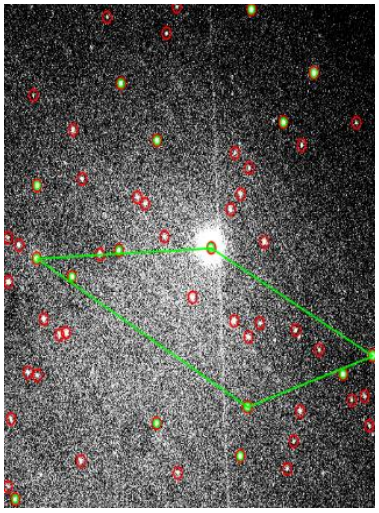

Fig. 3. Object segmentation and a sample quad formation

C. Photometric Analysis

After converging on an optimal solution for attitude, we utilized the catalog stars to estimate the apparent magnitude of the target satellite. For that purpose, we selected the magnitudes of neighboring stars to compute the apparent magnitude of the target satellite using the Pogson method. The Pogson method calculates the difference in brightness between two stars, expressed in magnitudes.

$$m_2 - m_1 = -2.5 \log\left(\frac{F_2}{F_1}\right) \quad (1)$$

where m_1 and m_2 are the magnitudes of two stars, and F_1 and F_2 are their fluxes (amounts of light energy). Here, we employed pixel brightness to estimate star and satellite fluxes. Additionally, the apparent magnitudes of each star were determined after registering them with the reference catalog. For each pair of stars and satellite, apparent magnitude was estimated using the Pogson method. Finally,

we took the average of the estimations for all star-satellite pairs to get the final estimate.

D. Determination Object Size

The Pogson Method is applied to satellites and space debris, and the Sun is taken as the reference brightness (2). The apparent visual magnitude of the Lambertian sphere is then given by

$$m_v = -26.74 - 2.5\log(A\rho F(\varphi)) + 5.0\log(R) \qquad (2)$$

where -26.74 is the apparent visual magnitude of the Sun [2].

The fraction F of incident solar flux is reflected by the spherical satellite as a function of phase angle, ϕ, A is the cross-sectional area, ρ is object's albedo, and R is the range between the observation site and the space object.

The flux value of the observed space object depends on its angle to the Sun (phase angle), reflection coefficient (albedo), and the assumed spherical radius of the object. Using equation (2), the space object size was calculated using the estimated observation magnitude and orbital parameters. Since the reflection model of the observed space object is unknown, 0.1, the albedo value used in the literature, was used in the calculations [13].

E. Observation

SJ-6F is a Chinese satellite launched in 2008 at an altitude of 585 km to examine the space environment, having a NORAD ID of 33409 (Radar Cross Section area: 2.21 m^2)[1]. We continuously observed the satellite with different optical systems at three sites (Site-1, Site-2, and Site-3). Site-1 had the best observation conditions according to the astronomical seeing and technical specifications of the optical systems compared to the others. Site-2 is located in a sparse settlement and sky brightness is 19^m. The average distance between Site-1 and Site-2 is 500 km. Site-3 is same location as Site-1 and had similar astronomical seeing conditions to Site-1; however, the specification of its optical system's quality was lower than Site-1. TABLE includes the details of the observations taken for this study.

TABLE I. OBSERVATION SITE AND OPTICAL SYSTEM FEATURES

Observation Site	Sky Magnitude (m)	Optical Aperture (cm)	Observation Date	Observation Number
Site-1	21	50-100	15.09.2022	36
			16.09.2022	75
			17.09.2022	97
			11.10.2022	42
			12.10.2022	33
Site-2	19	30-40	11.10.2022	58
			12.10.2022	17
Site-3	21	20-35	16.09.2022	11
			17.09.2022	9

The estimated observation and model-based magnitudes of SJ-6F for five different nights at Site-1 are shown in Fig. *4*, Fig. *5*, Fig, Fig. and Fig. . The magnitude values rise with the increase of elevation angles during the satellite's pass. We also observed that the estimated observation and model-based magnitudes were very close. On the other hand, the trends of the estimated observation and the model-based magnitudes are similar to the observations on Site-2 (Fig. *9* and Fig. *10*); however, their magnitude values are scattered over a wider area. Contrary to this, we observed a dissimilarity between the estimated observation and model-based magnitudes on Site-3 observations (Fig. and Fig.).

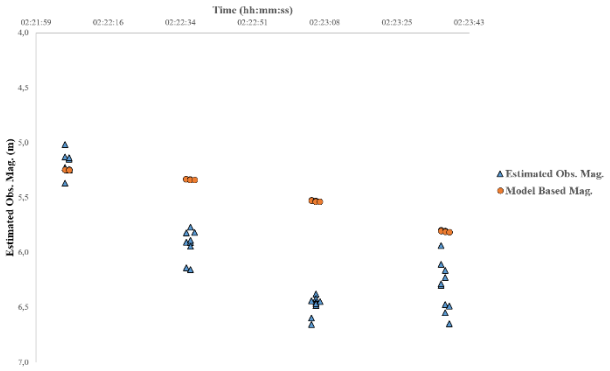

Fig. 4. Observation results in 15/09/2022 on Site-1

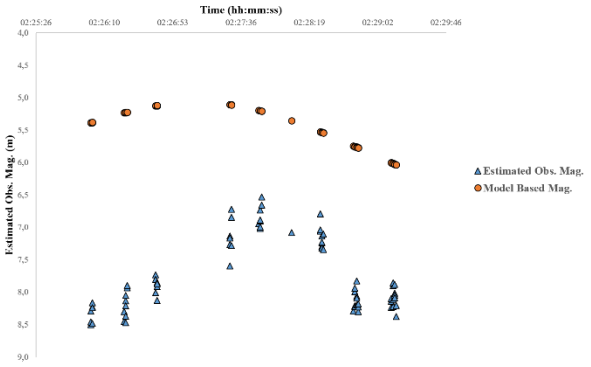

Fig. 5. Observation results in 16/09/2022 on Site-1

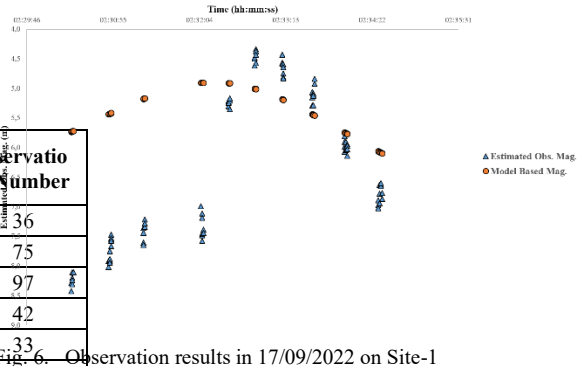

Fig. 6. Observation results in 17/09/2022 on Site-1

[1] SJ-6F satellite's information: https://www.n2yo.com/satellite/?s=33409

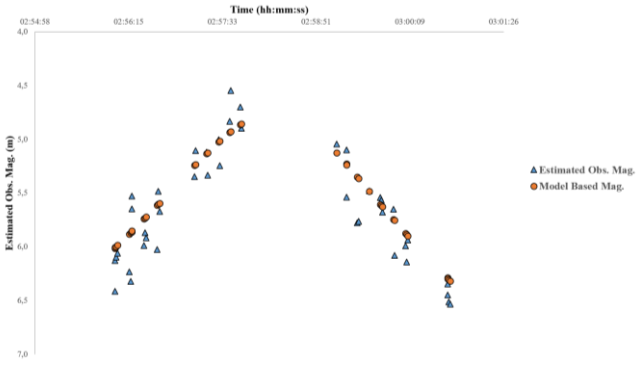

Fig. 7. Observation results in 11/10/2022 on Site-1

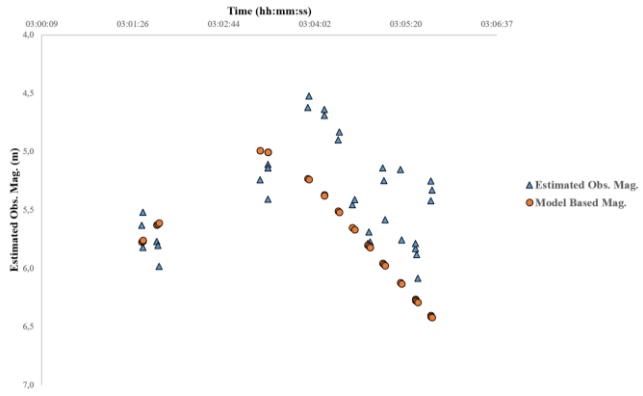

Fig. 8. Observation results in 12/10/2022 on Site-1

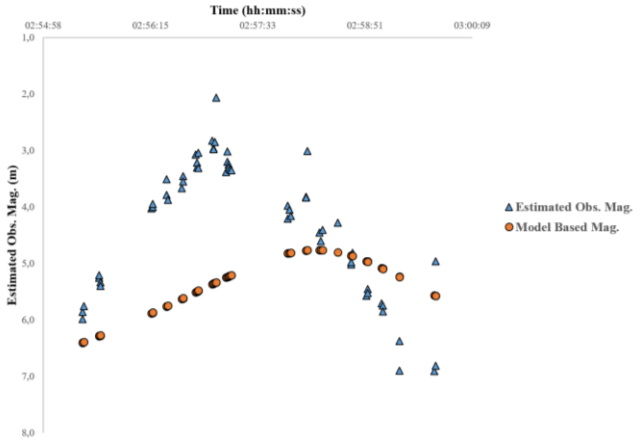

Fig. 9. Observation results in 11/10/2022 on Site-2

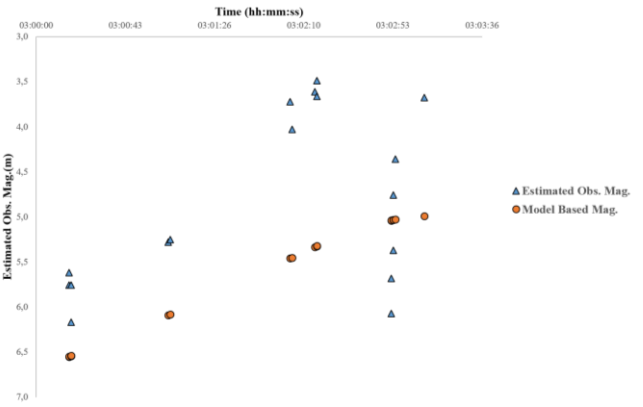

Fig. 10. Observation results in 12/10/2022 on Site-2

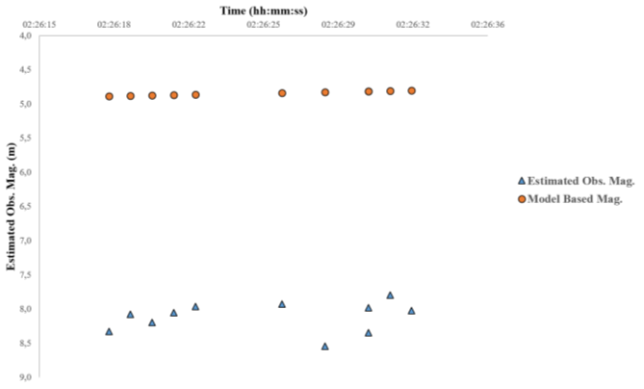

Fig. 11. Observation results in 16/09/2022 on Site-3

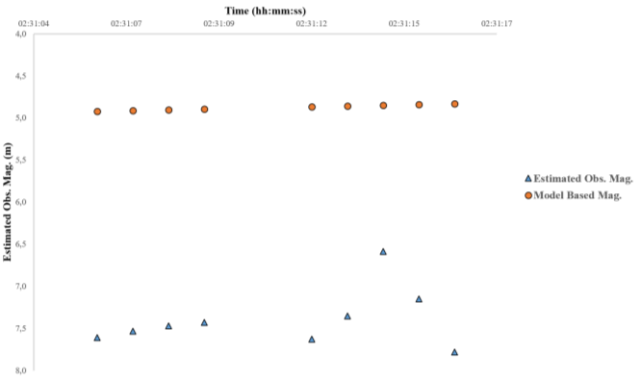

Fig. 12. Observation results in 17/09/2022 on Site-3

Additionally, we collected all the observations related to the selected satellite, as shown in Fig. and Fig. . In these results, we evaluated the estimated observation magnitude-range and the estimated observation magnitude-elevation graphs. The results clearly showed that estimating the observation magnitudes during the passes at low elevations highly deviates from the model-based magnitudes. On the other hand, the difference between the estimated observation and model-based magnitude values tends to be greater for the observations taken from Site-2 and Site-3.

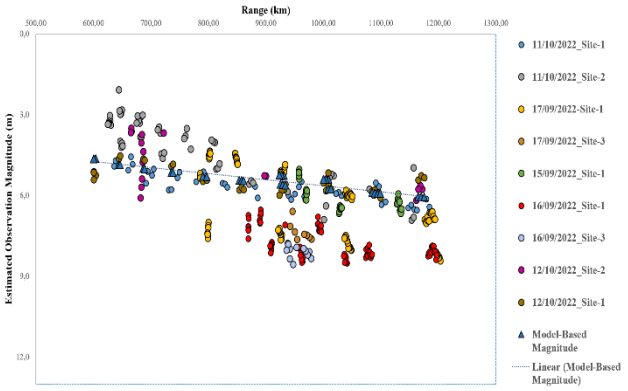

Fig. 13. Estimated Observation Magnitude - Range Chart

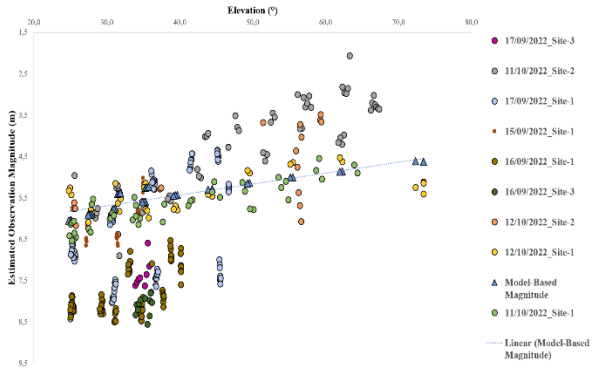

Fig. 14. Estimated Observation Magnitude - Elevation Chart

The brightness sensitivity measured on the images decreases due to the fact that the observation data is affected by the atmosphere at low elevations on satellite passes (Fig. and Fig.). On the other hand, the characteristics of the optical system and the background noise of the observation site affect the observation measurements. We realized that the values between the observed and model-based magnitudes were highly consistent for the observations above 45° in elevation for 11/10/2022 and 12/10/2022 taken from Site-1. Therefore, we filtered out the other observations and performed a linear regression analysis to get a linear estimation model in (3). Sample points of measurement and the model output are shown in Figure 15.

$$y = -0.0426x + 7.3698 \quad (3)$$

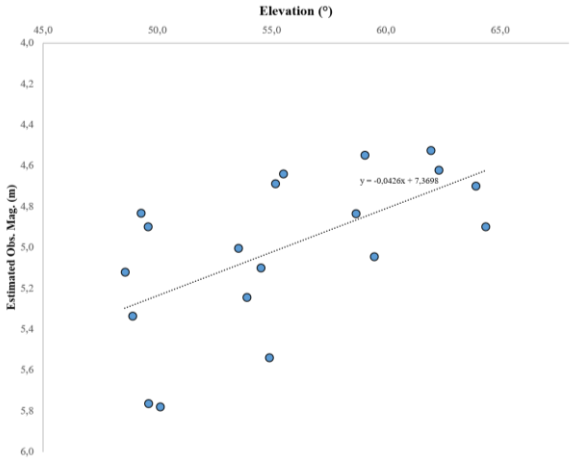

Figure 6 Estimated Observation Magnitude Trend up to 45° elevations on Site-1

In (3), the formulated magnitude is calculated using the elevation values at the time of observation by x (Table 2). By using these values in place of the brightness observed in (2), the cross-section area values are obtained at the time of observation. The calculated radius of the satellite dimension is obtained using (4). The formula,

$$\text{Cross Section Area} = \frac{4\pi r^2}{2} \quad (4)$$

where r is symbolized radius.

TABLE II. CALCULATED DIMENSION RESULTS OF THE OBSERVED SATELLITE

Time (dd/mm/yyy hh:mm:ss)	Obs Mag (m)	Cal Mag (m)	Elevation (°)	Range (km)	Formulated Mag (m)	Phase Angle (rd)	Cross Section Area (m)	Calculated radius (m)
11/10/2022 2:57:20	5,12	4,76	48,58	749,36	5,30	1,49	0,58	0,30
11/10/2022 2:57:21	5,33	4,75	48,91	746,11	5,29	1,48	0,58	0,30
11/10/2022 2:57:30	5,00	4,65	53,54	704,68	5,09	1,45	0,63	0,32
11/10/2022 2:57:31	5,24	4,65	53,91	701,79	5,07	1,45	0,64	0,32
11/10/2022 2:57:39	4,83	4,56	58,68	667,82	4,87	1,42	0,71	0,34
11/10/2022 2:57:40	4,55	4,56	59,08	665,34	4,85	1,42	0,72	0,34
11/10/2022 2:57:48	4,70	4,49	63,93	638,26	4,65	1,38	0,82	0,36
11/10/2022 2:57:49	4,90	4,48	64,35	636,20	4,63	1,38	0,83	0,36
11/10/2022 2:59:08	5,04	4,75	59,48	660,64	4,84	1,16	0,88	0,37
11/10/2022 2:59:16	5,54	4,86	54,90	691,33	5,03	1,16	0,81	0,36
11/10/2022 2:59:16	5,10	4,87	54,52	694,20	5,05	1,16	0,80	0,36
11/10/2022 2:59:25	5,78	4,98	50,12	731,01	5,23	1,16	0,75	0,35
11/10/2022 2:59:26	5,76	4,99	49,60	735,84	5,26	1,16	0,74	0,34
12/10/2022 03:03:56	4,62	4,86	62,31	644,52	4,72	1,01	1,08	0,41
12/10/2022 03:03:57	4,52	4,86	61,96	646,37	4,73	1,01	1,07	0,41
12/10/2022 03:04:10	4,64	5,00	55,51	686,65	5,00	1,00	0,94	0,39
12/10/2022 03:04:10	4,69	5,00	55,17	689,15	5,02	1,00	0,93	0,39
12/10/2022 03:04:22	4,90	5,14	49,60	735,66	5,26	1,01	0,85	0,37
12/10/2022 03:04:23	4,83	5,15	49,28	738,69	5,27	1,01	0,85	0,37

The radius was calculated using the measurements on Site-1 above 45° elevation was averaged, and the satellite's radius was founded as 0.356 meters. The radius of the satellite, calculated from the published magnitude of the satellite using equations (2) and (4), is 0.327 meters[2].

III. CONCLUSION

Earth orbit missions are used in many areas today. The increasing number of these missions affects space traffic. In Space Situational Awareness (SSA) research, satellites and space debris are cataloged using different systems, and precautions are taken with early warning systems for active missions.

On the other hand, space debris can fragment over time. In this study, we proposed a method to estimate the size of celestial objects according to their observed brightness values through passive optical systems. For that purpose, we observed a satellite object with a known size at different times from various locations. The results showed that the estimation accuracy depends on light pollution, atmosphere effect, elevation angle, and optical system characteristics. After eliminating low-accuracy results (at below 45° elevation), the average radius of the selected satellite (NORAD ID 33409) could be precisely calculated from the observations. The radius estimation from observations is 0.356 meters, while the radius of the satellite is 0.327 meters.

In future studies, it is aimed to obtain a more accurate dimensional analysis from the brightness by observing the satellite or space debris whose size is known directly.

[2] NORAD ID: 33409 satellite's published brightness https://www.heavensabove.com/satinfo.aspx?satid=33409

REFERENCES

[1] H. Krantz, E. C. Pearce and A. Eric C, "Characterization of LEO Satellites With All-Sky Photometric Signatures," 2022.

[2] R. Cognion, "Observations and Modeling of GEO Satellites at Large Phase Angles," in *Advanced Maui Optical and Space Surveillance Technologies Conference*, 2013.

[3] J. Šilha, M. Zigo, T. Hrobár, P. Jevčák and M. Verešvárska, "Light Curves Application to Space Debris Characterization and Classification," 2021.

[4] R. Linares, R. Furfaro and V. Reddy, "Space Objects Classification via Light-Curve Measurements Using Deep Convolutional Neural Networks," 2018.

[5] M. Hejduk, H. Cowardin and E. Stansbery, "Satellite Material Type and Phase Function Determination in Support of Orbital Debris Size Estimation," 2012.

[6] D. Hall, B. Calef, K. Knox, M. Bolden and P. Kervin, "Separating Attitude and Shape Effects for Non-resolved Objects," 2007.

[7] F. Piergentili, G. Zarcone, L. Parisi, L. Mariani, S. H. Hossein and F. Santoni, "LEO object's light-curve acquisition system and their inversion for attitude reconstruction," *Aerospace,* vol. 8, p. 4, 2020.

[8] H. M. Cowardin, J. A. Reyes, E. A. Plis, R. C. Hoffmann, G. P. Badura, J. R. Shah, S. E. J. Collman, M. T. Bengtson, D. P. Engelhart and T. R. Scott, "Spectral Characterization of Modern Spacecraft Materials," 2022.

[9] M. Nussbaum, E. Schafer, Z. Yoon, D. Keil and E. Stoll, "Spectral Light Curve Simulation for Parameter Estimation from Space Debris," 2022.

[10] H. Cowardin, K. Abercromby, S. E. Barker and T. Schildknecht, "Characterization of Orbital Debris Photometric Properties Derived from Laboratory-Based Measurements," 2010.

[11] K. Abercromby, K. S. Jarvis and E. S. Barker, "Using Light Curves to Characterize Size and Shape of Pseudo-Debris," 2006.

[12] J. Africano, P. Kervin, D. Hall, P. Sydney, J. Ross, T. Payne, S. Gregory, K. Jorgensen, K. Jarvis, T. Parr-Thumm, G. Stansbery and E. Barker, "Understanding Photometric Phase Angle Corrections," 2005.

[13] H. Seo, H. Jin, Y. Song, Y. Lee and Y. Oh, "The Photometric Brightness Variation of Geostationary Orbit Satellite," 2013.

[14] B. Schmalzel, "The Feasibility and Application of Observing Small LEO Satellites with Amateur Telescopes," 2013.

[15] D.-G. Roh, J. Choi, J. Jo, H.-S. Yim, S.-Y. Park, M. Park, Y.-J. Choi, Y.-H. Bae, Y. Park, H.-J. Jang, S. Cho, J.-H. Kim and J.-H. Park, "Magnitude Standardization Procedure for OWL-Net Optical Observations of LEO Satellites," *Journal of Astronomy and Space Sciences,* vol. 32, pp. 349-355, December 2015.

[16] G. Bradski, "The OpenCV Library," *Dr. Dobb's Journal of Software Tools,* 2000.

[17] N. Zacharias, C. T. Finch, T. M. Girard, A. Henden, J. L. Bartlett, D. G. Monet and M. I. Zacharias, *The fourth U.S. Naval Observatory CCD Astrograph Catalog (UCAC4),* 2012.

[18] D. Lang, D. W. Hogg, K. Mierle, M. Blanton and S. Roweis, "Astrometry. net: Blind astrometric calibration of arbitrary astronomical images," *The astronomical journal,* vol. 139, p. 1782, 2010.